Shifts in mutation spectra enhance access to beneficial mutations

Mrudula Sane[1], Gaurav D Diwan[1,2,3], Bhoomika A Bhat[1,4], Lindi M Wahl[5]* and Deepa Agashe[1]*

[1] National Centre for Biological Sciences, GKVK Campus, Bellary Road, Bengaluru, India

[2] CellNetworks, Bioquant, University of Heidelberg, 69120 Heidelberg, Germany

[3] Biochemie Zentrum Heidelberg (BZH), University of Heidelberg, 69120 Heidelberg, Germany

[4] Undergraduate Programme, Indian Institute of Science, Bengaluru, India

[5] Western University, London, Ontario, Canada

*Correspondence to:

dagashe@ncbs.res.in

lwahl@uwo.ca

ABSTRACT

Biased mutation spectra are pervasive, with widely varying direction and magnitude of mutational biases that influence genome evolution and adaptation. Why are unbiased spectra rare, and how do such diverse biases evolve? Our experiments show that changing the mutation spectrum allows populations to sample previously under-sampled mutational space, including new beneficial mutations. The resulting shift in the distribution of fitness effects is advantageous: beneficial mutation supply and beneficial pleiotropy both increase, and deleterious load reduces. More broadly, adaptive walk simulations indicate that the evolution of a mutational bias in an unbiased ancestor is selectively neutral; but reversing the direction of a long-term bias is always selectively favoured. Indeed, spectrum changes in the bacterial phylogeny occur frequently, typically involving reversals of ancestral bias. Thus, shifts in mutation spectra may evolve under selection, and can directly alter the outcome of adaptive evolution by facilitating access to beneficial mutations.

SIGNIFICANCE STATEMENT

Mutations are important because they provide raw material for evolution. Some types of mutations occur more often than others, but the direction and degree of such mutational biases varies. How do mutational biases evolve, and do they influence evolution? We experimentally measured the immediate effects of changing the mutation bias of *E. coli*, and used simulations to test the long-term effects. Altering mutational bias is beneficial whenever the new bias increases sampling of mutational classes that were previously under-sampled. We also show that historically, bacteria have often experienced such beneficial bias switches. Our work demonstrates the importance of mutational biases in evolution. By allowing exploration of new mutational space, altered mutation biases could drive rapid adaptation even in constant environments.

INTRODUCTION

The mutation spectrum describes the frequency of various classes of sampled mutations (e.g. transversions vs. transitions (Tv/Ts)), and is often determined by the action of DNA repair enzymes. Changes in DNA repair function typically alter both mutation rate and spectrum, e.g. in "mutator" genotypes with loss-of-function mutations (1), or during stress-induced mutagenesis (2, 3). By determining the pool of genetic variants available for selection, mutation spectra can shape key genome features (e.g. nucleotide (4, 5), codon and amino acid composition (6)), even under selection for thousands of generations (7); determine the genetic basis of adaptation (8–12), driving convergent evolution (13–15); and shape the evolution of resistance to antibiotics (16–18) and anti-cancer drugs (19). Thus, mutation spectra are important for adaptive evolution; but their role is underappreciated (8).

Most species have a skewed mutation spectrum, with substantial variation in the direction and magnitude of bias (20, 21) (experimental data for microbes summarized in Table S1). This diversity implies major evolutionary shifts in mutation spectra. However, the frequency, underlying evolutionary processes, and consequences of spectrum shifts are unknown. For instance, why are unbiased spectra rare? Do spectrum shifts – for example, a change from an unbiased to a biased state, or altered direction of bias – evolve under selection? A spectrum shift may persist if the new bias favours mutational classes that are inherently advantageous (8, 22), allowing the evolved bias to hitchhike with beneficial mutations. It has also been speculated that stress-induced changes in mutation spectra may enhance sampling of new beneficial mutations by altering the distribution of fitness effects (DFE) (23, 24). However, prior studies have failed to find consistent support for generalized selective benefits of specific mutational classes. For instance, transition mutations are not consistently more beneficial (or less deleterious) than transversions (25, 26); and the fixation probability of Ts vs. Tv mutations in genomes is clade-specific (27). Hence, particular mutational classes do not seem to be universally beneficial, and the observed diversity in mutation bias remains puzzling.

We addressed these gaps using a combination of experiments, simulations, and phylogenetic analyses. To measure the immediate evolutionary impact of the mutation spectrum, we estimated the genome-wide DFE of new mutations in *Escherichia coli*. We manipulated the mutation spectrum by deleting a DNA repair gene (Δ*mutY*, "mutator") from our wild type ("WT") strain, altering both the mutation spectrum and rate (1). Allowing independent lineages of both strains to evolve under mutation accumulation (MA), we sequenced whole genomes of evolved isolates to identify strains carrying a single new mutation each. Thus, we minimized the impact of selection on the mutation spectrum and the DFE, while also decoupling the effects of the mutator's spectrum from its high mutation rate. Measuring the effect of each single mutation on population growth rate, we determined the effects of mutation spectrum on the beneficial mutation supply, genetic load, and pleiotropic effects. Next, to test the generality and longer-term evolutionary consequences of shifts in mutation spectra, we simulated adaptive walks across NK fitness landscapes (28). Finally, we inferred evolutionary transitions in DNA repair enzymes across the bacterial phylogeny to estimate the frequency of shifts in mutation bias. Our results show that shifts in mutation spectra can evolve under selection and fuel adaptation via previously under-sampled evolutionary paths.

RESULTS AND DISCUSSION

The mutator DFE has more beneficial mutations that reduce the expected genetic load and alter pleiotropic effects

From MA experiments conducted in rich media (LB), we obtained 80 evolved WT (29) and 79 mutator strains, each carrying a single distinct mutation with respect to its ancestor (Supplementary Data). We measured the selective fitness effect (relative growth rate) of each mutation in the MA environment (LB) as well as 15 other environments with different carbon sources, including some that are used by *E. coli* in the mouse gut (30). With this large set of fitness effects, we constructed environment-specific empirical DFEs (WT data were previously reported (29)). Since bacterial MA experiments can cause over-sampling of beneficial mutations and under-sampling of deleterious mutations, we used a correction method (31) that retains the measured selective effect (s) of each

mutation, but estimates and corrects for selection bias by changing the frequency of mutations with a given selective effect (Fig. S1A–C, Supplementary Data). These corrected DFEs thus provide accurate estimates of the fraction of beneficial mutations (f_b) and the average selective effect (s).

The bias correction results in DFEs with coarsely binned fitness histograms, which we used to calculate the fraction of neutral ($-0.05 < s < 0.05$, conservatively accounting for a maximum of ~5% fitness measurement error), beneficial ($s > 0.05$), and deleterious ($s < -0.05$) mutations for each strain in all 16 environments. Fisher's geometric model predicts that in well-adapted populations, f_b should be low, but should approach 50% when populations are poorly adapted (37). Indeed, in LB (rich medium) the WT and mutator had the lowest f_b (~5%, Fig. 1). However, overall f_b was not correlated with ancestral fitness across environments in either strain (Spearman's rank correlation test, WT: rho = -0.217, Mutator: rho = -0.18; $p > 0.05$ in each case). On average, the mutator had a greater fraction of beneficial mutations than the WT (f_b = 36% vs. 28%), but fewer deleterious mutations (Fig. 1, Table S2). Thus, compared to WT, the mutator had more beneficial-shifted DFEs. Mean fitness effects of mutations were also significantly more beneficial in the mutator (paired Welch's two-sample test, $p = 0.043$; Fig. S2A), although medians were not significantly different ($p = 0.35$, Fig. S2B). Finally, mutations had larger absolute effects in WT than in the mutator (Wilcoxon's rank-sum test, $W = 662920$, $p = 1.4\times10^{-14}$); hence, the mutator's beneficial-shifted DFEs could not have arisen because of overall larger-effect mutations. These results indicate a broad selective advantage to the mutator, independent of its mutation rate. In addition, accounting for the skewed DFEs and order-of-magnitude higher mutation rate ($\mu_{WT} = 9.3\times10^{-11}$ per bp per generation, $\mu_{mutator} = 89\times10^{-11}$, Table S3), we estimated (following (45)) that on average the mutator should have an ~16-fold greater genome-wide supply of beneficial mutations, and ~6-fold higher genetic load than the WT (Tables S4, S5). In contrast, if we ignored the mutator's distinct DFE and accounted only for its mutation rate, both the supply of beneficial mutations and the deleterious genetic load would be nearly 10-fold greater than WT (Tables S4, S5). Thus, depending on their mutation rate and DFE, mutators may have a substantially higher supply of beneficial mutations and smaller genetic load than previously believed.

The high f_b values we observe (Fig 1) contradict the general expectation that beneficial mutations should be rare (32). However, many other studies – including with microbes and plants – have also reported a large number of beneficial mutations (33–39). The large f_b has been partially attributed to an improved ability to measure small-effect beneficial mutations (36, 40, 41) that are more common than expected (42), especially at low effective population sizes (38). We also note that most prior studies (32) provide approximate or indirect estimates of the DFE, by random mutagenesis of a single gene, focusing only on the beneficial part of the DFE, or inferring the DFE by fitting a model to time series data from selection or MA lines. Further, they do not estimate the number of underlying mutations to account for epistasis. Our direct, genome-wide estimates of the DFE of single, randomly-sampled new mutations support the idea (43, 44) that new beneficial mutations may be more common than generally believed.

Next, we estimated the pleiotropic effects of mutations (Fig. 2A), which are important because they can facilitate adaptation (via synergistic pleiotropic benefits) and shape fitness tradeoffs (via antagonistic pleiotropy) in new environments. The mutator had a distinct distribution of pleiotropic effects in all 16 environments (compare Fig. S2C and S2D, Table S6), driven by a higher incidence of beneficial synergistic pleiotropy and lower deleterious synergistic pleiotropy. However, both strains had similarly low antagonistic pleiotropy (Fig. 2B–C). Beneficial mutations in the mutator were also beneficial across many more environments (KS test, D=0.41, $p=3.1\times10^{-6}$); whereas deleterious mutations were deleterious in fewer environments than WT (KS test, D=0.56, $p=2.63\times10^{-11}$) (Fig. 2F, Fig. S3). Thus, new beneficial mutations in the mutator are more likely to facilitate adaptation across many environments, but are no more likely to generate tradeoffs. Interestingly, simulating an increase in the median fitness effect of the WT DFE without changing its shape ("WT-beneficial shift") mimicked pleiotropic effects observed in the mutator in all but two environments (Fig. 2D, Fig. S2E, Table S6). Conversely, simply reducing the median fitness effect in the WT DFE ("WT-deleterious shift") lowered beneficial synergistic pleiotropy in all 16 environments (Fig. 2E, Fig. S2F, Table S6). Ignoring the mutation spectrum can thus cause overestimation of a mutator's genetic load, and underestimation of the supply and pleiotropic effects of beneficial mutations.

The mutator's beneficial-shifted DFEs arise from its distinct mutation spectrum

We had hypothesized that the mutator's distinct DFE could arise from its biased spectrum. However, other global effects of the initial *mutY* gene deletion could also lead to a DFE shift. For instance, if deleting *mutY* reduced the mutator's fitness, a larger fraction of new mutations might be beneficial (46). However, the mutator ancestor had lower fitness than WT in only three environments (Fig. 3A, Table S7). Alternatively, epistatic interactions with *mutY* could increase the deleterious effect of new mutations in the WT. However, paired WT and mutator strains carrying the same mutation had similar fitness in all but one environment (Fig. 3B, Table S8). Thus, the observed shift in the mutator DFE cannot be explained by global effects of the *mutY* deletion. The difference across strains was also robust across mutational classes: mutations were more beneficial in the mutator even when comparing only coding, synonymous, or non-synonymous mutations (Fig. S4).

Next, we asked whether the mutator over-samples mutational classes that happen to be more beneficial (or less deleterious). The mutator strongly favours transversions, GC→AT mutations, base pair substitutions (BPS) and coding mutations (Fig. 3C, Table S3). The resulting skew in sample size limited our ability to directly test the association between mutation bias and fitness effects across strains. However, in the WT (where sampling of mutational classes was balanced), transversions and GC→AT mutations were indeed less deleterious than transitions and AT→GC mutations (Fig. 3D–E; fitness effects pooled across environments, Table S9; for other biases, see Fig. S4, Table S9). In contrast, other aspects of the mutations (e.g., genomic location or specific amino acid changes) did not differ across strains (Fig. S5 and S6; Tables S10, S11). Thus, as predicted, the mutation spectrum – specifically the strong Tv and GC→AT bias – appeared to drive the distinct DFE of the mutator. However, it was unclear why Tv and GC→AT mutations should be more beneficial.

Simulations demonstrate a general benefit of reversing mutation spectra

To test the generality of our empirical results and uncover underlying mechanisms, we simulated adaptive walks (following (47)), modelling sequences of N nucleotides such that mutations could be classified as Ts vs. Tv or GC→AT vs. AT→GC. Starting from a randomly chosen ancestor sequence and mutation spectrum (Tv bias = fraction of transversions), we allowed populations to explore successive mutational steps at randomly chosen loci (bases). A mutation that confers a relative fitness increase of 1+s immediately fixes (a step in the walk is taken) with probability 2s; that is, we assumed a strong-selection weak-mutation regime. At various points during the walk, we simulated mutations to generate a DFE, computed fitness effects given the underlying fitness landscape (affected by K other randomly chosen loci, to incorporate epistasis), and calculated the fraction of beneficial (f_b) and deleterious (f_d) mutations and their effect sizes. We initially set N=200 and K=1 (each locus epistatically coupled to 1/199=0.5% loci), and present the average outcomes for 500 adaptive walks on 500 randomly-generated fitness landscapes (Fig. S7A–B shows variation across walks).

As expected, mean population fitness increased during the adaptive walk, with a concomitant reduction in f_b and beneficial effect size, an increase in f_d, and a relatively constant deleterious effect size (Fig. 4A). Setting ancestral Tv bias to 0.45 (mimicking our WT), we compared the DFE generated by the ancestor at various time points, to the DFE that would be created if the bias were changed (mimicking our Δ*mutY* strain). The bias-shifted ("shifted") strain thus started with the same fitness and sequence as the ancestor and an identical mutation rate, differing only in spectrum. As the population evolved (i.e. ancestor f_b decreased), a stronger bias shift (i.e. higher Tv) allowed the sampling of proportionally more beneficial mutations than the ancestor (Fig. 4B). More generally, exploring well-adapted populations (f_b = 0.04) but varying both the ancestral and shifted mutation spectra, we find that shifted strains that reverse the ancestral bias (i.e., have a strong bias in the opposite direction) have the greatest advantage (Figs. 4C–4F). These results hold even with a different axis of the mutation spectrum (GC→AT bias, Fig. S7C–H) or in more rugged fitness landscapes with higher epistasis (Fig. S8A–B). Importantly, the adapting populations did not "exhaust" a small set of beneficial mutations; rather, they fixed distinct mutations as they explored

a large number of diverse pathways that represent a subset of many possible fitness peaks (Fig. S8C).

Thus, our simulation results can be broadly generalized as follows: (1) reversing an existing mutation bias is always beneficial (2) the magnitude of the benefit increases with the degree to which the new bias opposes the ancestral bias, and (3) the magnitude of the benefit increases when the ancestor has evolved with a fixed bias for longer intervals of time (i.e. as the ancestor gets better-adapted over time). Our experimental data with the Δ*mutY* strain support the first prediction, but appear to contradict prediction 3, in that the largest difference in f_b between WT and mutator in not observed in LB (where ancestral growth rate is highest and presumably *E. coli* is best-adapted). Note however, that because absolute growth rate is strongly influenced by nutrient availability, it is not a reliable indicator of the relative degree or time of adaptation to a specific environment. Hence, predictions 2 and 3 must be tested explicitly in further work, under conditions where the degree of bias change and the length of evolutionary time in an environment are known. Additionally, although our Δ*mutY* mutator reversed the WT Tv bias (explaining Fig. 3D), it reinforced the WT GC→AT bias, rendering the results in Figure 3E puzzling. However, ~88% of all GC→AT mutations in the mutator are also transversions. Hence, our mutator's observed beneficial-shifted DFE is explained by its strong Tv bias, which opposes the existing WT bias towards Ts.

The results above demonstrate general conditions under which a change in mutational bias can be selectively advantageous. But how does mutation bias evolve in the first place, from an unbiased state? Starting from an unbiased ancestor (Tv bias = 0.66 since 2/3 of possible mutations are transversions), we find that introducing any bias is selectively neutral, regardless of how long the ancestor had evolved in the same fitness landscape (Fig. 4G–H). However, if the ancestor had previously evolved with a biased spectrum (e.g. our WT), the population would have over-sampled beneficial mutations within the class favoured by the existing bias. Hence, a shift in the opposite direction (e.g. in our Δ*mutY* strain) allows the population to explore mutational space that was previously under-sampled, increasing the probability of finding new beneficial mutations.

Importantly, this means that the benefit of a specific mutation class (e.g. Tv) is not universal, but is context-dependent. Increased sampling of any mutational class that was previously poorly explored would therefore be beneficial. Thus, after a period of evolving with a new spectrum, a change in the fitness landscape (e.g. due to epistasis or environmental change) may again render a spectrum shift advantageous. Together, these results generate two broad predictions: (a) starting from an unbiased spectrum, a biased spectrum can only evolve through drift, and (b) after a period of adaptation with a specific mutation bias (and/or following environmental change), reversing the bias becomes beneficial.

Evolutionary transitions in DNA repair enzymes indicate mutation spectrum reversals in most bacterial lineages

Altering DNA repair function is a simple and instantaneous mechanism to generate spectrum shifts. Hence, to infer long-term mutation spectrum dynamics we mapped evolutionary transitions in 11 bacterial DNA repair enzymes whose loss changes the Tv or GC→AT bias in *E. coli* (Table S12). Identifying gene orthologues in 1093 extant bacterial genomes, we used ancestral reconstruction to infer enzyme gains and losses across a pruned tree derived from a previously published whole-genome bacterial phylogeny based on >400 proteins (following (48); Fig 5A). Broadly consistent with previous work with a few DNA repair genes (49), we found frequent evolutionary transitions in most repair enzymes. Using the predicted set of enzymes for hypothetical ancestors (nodes), we estimated their Tv and GC→AT bias relative to WT *E. coli* and traced the change in relative bias over time (Fig. 5B, Fig. S9A). Consistent with our model results, successive enzyme gain or loss events led to a bias reversal in >80% lineages, and we observed only a few cases of reinforced bias (Fig. 5C). This is distinct from the pattern expected by chance (stochastic simulations using similar enzyme transition rates; Fig. 5C, Fig. S9B). Notably, single reversals in Tv bias and double reversals in GC→AT bias were more frequent than expected (Tv bias: χ^2=805.3, $p<2x10^{-16}$; GC→AT bias: χ^2=453.5, $p<2x10^{-16}$; Fig. 5C, Fig. S9B). Hence, our results cannot be attributed to peculiarities of the enzyme set, tree topology, or number of evolutionary transitions. Instead, we suggest that such frequent bias reversals likely reflect selection on mutation rate and/or spectrum.

While it is difficult to separate these effects, note that enzymes with a weak effect on the mutation rate but a strong impact on the spectrum are also highly dynamic (e.g. *ung* and *mutM*; Table S12). Interestingly, 33 additional genes from multiple DNA repair modules also show frequent evolutionary transitions (Fig. S10).

We discuss here a few limitations of this analysis. First, reconstruction of ancestral character states in phylogenetic datasets is not always accurate (50). Second, the estimated biases do not account for other repair enzymes whose effects on the mutation spectrum are unknown, and for variation in the impact of enzyme loss. Given the lack of empirical data for most bacteria, the values we report are our best estimates of the mutation biases of diverse bacteria relative to *E. coli*. However, available data show that the effects of deleting a DNA repair enzyme are largely consistent across species (Table S13), suggesting that the broad trends observed here should be robust. Finally, recent work by others also indicates similar dynamics of genes involved in DNA repair in bacteria (51) and fungi (52). Thus, sustained shifts in mutation spectra likely occur frequently, and their potential long-term impacts on the pool of genetic variants available for selection deserve further investigation.

CONCLUSIONS

We show that pervasive mutational biases can evolve by genetic drift, whereas shifts in the strength and direction of bias could evolve under selection. Thus, a species' evolutionary history may be sufficient to explain the evolution of genomic bias (e.g. in base composition), without invoking specific underlying mechanisms or selection favouring particular mutational classes. Our model also explains recent observations that GC-biased mutations in protein-coding genes are more deleterious in GC-rich genomes, and vice versa (53); such symmetrical results are otherwise difficult to explain. By recasting the puzzle of mutational biases as a problem of searching a vast and dynamic mutational space, our model allows broad generalization across mutation spectra. Here, we simulated a strong selection weak mutation regime; we speculate that bias shifts may be even more favored under clonal interference by allowing access to rare beneficial mutations of

large effect. Full population simulations with multiple segregating mutations would offer further insight into such a strong mutation regime. We suggest that the rarity of species with unbiased mutation spectra (21) is counterintuitive but not surprising, since transitions from unbiased to biased spectra may occur easily and frequently via changes in DNA repair function. Hence, a biased spectrum should be the norm rather than the exception.

Our results indicate that shifts in mutation spectra and mutation rates are deeply entangled due to their strong association with mutator genotypes, whose evolutionary dynamics are governed by the genetic load and supply of beneficial mutations (45, 54, 55). In a new environment (away from fitness optima), these parameters are primarily driven by mutators' high mutation rate (56)– particularly under strong selection (57) – allowing them to hitchhike with beneficial mutations (58). We show that the beneficial supply rate is strongly influenced by the mutation spectrum, and this effect is strongest in well-adapted populations. Further, the advantage of a high mutation rate should be enhanced if accompanied by a reversal of the ancestral spectrum; but diminished otherwise. Thus, mutation rate and spectrum may jointly govern the observed rise, persistence, and fall of mutators under selection (45, 59). These effects may explain why mutators with relatively small increases in mutation rate are also abundant in natural bacterial populations (60), and deserve further attention (53). Instances where spectrum shifts occur without a rate change – e.g. during stress-induced mutagenesis (20, 24) or the loss of repair enzymes like *ung* and *mutM* – offer a chance to untangle their evolutionary impacts. In particular, quantifying the effects of mutation spectrum and rate (as we have done here) in conjunction with selection experiments would allow better prediction of the evolutionary dynamics of specific types of mutators in diverse environments.

Together with studies showing that mutation biases are pervasive and influence the genetic basis of adaptation under diverse conditions (see Introduction), our results demonstrate that mutation spectra may be important drivers of adaptation and innovation under myriad scenarios. When the beneficial mutation supply is limited by the existing spectrum, an antiparallel (opposite direction on the same axis) or orthogonal jump (on a different axis of the spectrum) could enhance sampling of

new beneficial mutations, facilitating rapid adaptation. Our phylogenetic analysis likely underestimated such evolutionary shifts in mutation spectra, which may occur even more frequently on shorter timescales via horizontal transfer and recombination (61), and drive polymorphism in spectra across natural bacterial isolates (60, 62). We predict multiple cascading effects of shifts in mutation spectra, including a reduction in the waiting time for beneficial mutations, decreased likelihood of mutational meltdown under genetic drift, and distinct genetic pathways of adaptation. We hope that future work will test these predictions.

METHODS

Bacterial strains

We obtained the wild-type (WT) strain of *E. coli* K-12 MG1655 from the Coli Genetic Stock Centre (CGSC, Yale University), streaked it on LB (Luria Bertani) agar, and chose one colony at random as the WT ancestor for subsequent experiments. We similarly obtained the mutator strain of *E. coli* (Δ*mutY*) from the Keio collection (BW25113 strain background; (63)) of gene knockouts from the same stock centre. These gene knockouts were made by replacing open reading frames with a Kanamycin resistance cassette, such that removing the cassette generates an in-frame deletion of the gene. The design of gene deletion primers ensured that downstream genes were not disrupted due to polar effects (63). We moved the knockout locus from the BW25113 background into the MG1655 (WT) background using P1-phage transduction (64). We then removed the kanamycin resistance marker by transforming kanamycin-resistant transductants with pCP20, a plasmid carrying the flippase recombination gene and Amp^R resistance marker. We grew ampicillin resistant transformants at 42 ºC in LB broth overnight to cure pCP20. We streaked out 10 µL of these cultures on LB plates. After 24 hours, we replica-plated several colonies on both kanamycin-LB agar plates and ampicillin-LB agar plates, to screen for the loss of both kanamycin and ampicillin resistance. We PCR-sequenced the knockout locus to confirm removal of the kanamycin cassette. We used the same protocol to generate Δ*ung* and Δ*mutM* strains to determine their mutation spectra.

To test whether genetic background alters the fitness effects of single mutations observed during mutation accumulation (MA), we deleted the *mutY* locus from 19 evolved WT MA lines (see below). We raised P1 phage on the Δ*mutY*::kanR strain in the MG1655 genetic background and infected evolved WT MA lines to obtain unmarked Δ*mutY* strains carrying the evolved WT mutation, as above. We confirmed the *mutY* deletion by sequencing the *mutY* locus. Thus, for each of the 19 mutations, we obtained paired strains with either a WT or Δ*mutY* genetic background.

Experimental evolution under mutation accumulation (MA)

We founded 38 WT MA lines from 38 different colonies (two lines per Petri plate) incubated at 37ºC, as described earlier (29). For each line, every 24 hours we streaked out a random colony (closest to a pre-marked spot) on a fresh LB agar plate. Every 4-5 days, we inoculated a part of the transferred colony in LB broth at 37ºC for 2-3 hours and froze 1 mL of the growing culture with 8% DMSO at -80 ºC. For the current study, we used stocks frozen on days 39 (~1072 generations), 104 (~2860 generations), 140 (~3850 generations), 200 (~5500 generations), 250 (~6875 generations) and 300 (~8250 generations). For the mutator, we similarly founded 300 MA lines, and evolved them for 12 days (~330 generations). This time was expected to be sufficient for the accumulation of one mutation per line on average, based on previous estimates of mutation rate (1). We made stocks of all lines as described for WT. To determine the impact of two previously untested DNA repair enzymes (*ung* and *mutM*) on the mutation spectrum, we evolved 20 independent MA lines of each deletion strain for 160 days (~4400 generations) and 210 days (~5775 generations) respectively.

Whole-genome sequencing to identify single mutations and determine mutation spectra

We sequenced individual colonies from MA experiments to identify clones carrying only a single mutation relative to the WT or *ΔmutY* ancestor. For WT, we sequenced MA lines at days 39, 104, 140, 200, 250, 300 as described earlier (29), to obtain 80 single mutational steps that we used for the analyses in the present study. We sampled lines at different time points since each line acquired its first mutation at different time points. For *ΔmutY*, we sequenced whole genomes of the 300 colonies from the MA experiment frozen on day 12, and the Δ*mutY* MA ancestor. To do

this, we inoculated 2 µL of the frozen stock of each evolved MA line (or the ancestor) in 2 mL LB, and allowed the cells to grow overnight at 37ºC with shaking at 200 rpm. We extracted genomic DNA (GenElute Bacterial Genomic DNA kit, Sigma-Aldrich), quantified it (Qubit HS dsDNA assay, Invitrogen), and prepared paired-end libraries from each line using the Illumina Nextera XT DNA library preparation kit per the manufacturer's instructions. We sequenced the Δ*mutY* MA ancestor on the Illumina MiSeq platform using the 2x250bp paired-end reaction chemistry, and obtained a total of 1.2M reads with quality > Q30, corresponding to an average per base coverage of ~120x. We sequenced libraries from the evolved MA lines on the Illumina HiSeq 2500 platform using the 2x100bp paired-end reaction chemistry. We obtained sufficient reads for 299 out of the 300 samples (median 3.3 million reads per sample; range: 1.15 – 7.13 million reads per sample), which we retained for further analysis. We discarded reads with quality < Q30, obtaining a median per base coverage of ~92x (range: 32x – 198x). For each sample, we aligned quality-filtered reads to the NCBI reference *E. coli* K-12 MG1655 genome (RefSeq accession ID GCA_000005845.2) using the Burrows-Wheeler short-read alignment tool (65). We generated pileup files using SAMtools (66)and used VARSCAN to extract a list of base-pair substitutions and short indels (<10bp)(67). For further analysis, we only retained mutations with >80% frequency that were represented by at least 5 reads on both strands.

After removing ancestral mutations from the evolved lines, we identified 79 *ΔmutY* MA-evolved lines that each had a single new mutation compared to the ancestor. We performed all further experiments and analyses with our 80 WT and 79 *ΔmutY* isolates (see Supplementary data). To calculate mutation rates and estimate mutation spectra, we used mutations called from all sequenced isolates at day 300 for WT and day 12 for Δ*mutY*, irrespective of whether they had single or multiple mutations (total 237 mutations in WT and 669 in mutator). Similarly, we determined the mutation spectra of Δ*ung* and Δ*mutM* strains by sequencing 20 isolates per strain (total 157 and 138 mutations respectively). We calculated mutational biases from the fraction of different types of mutations observed in our evolved strains (Table S3). We calculated the WT Tv bias as the number of transversions/(number of transitions + number of transversions) = 0.447. Therefore, we used WT Tv bias = 0.45 for our adaptive walk simulations (Fig. 4). Similarly, we

calculated the WT GC→AT bias as the number of GC→AT mutations/(number of AT→GC mutations + number of GC→AT mutations) = 0.59 (ignoring 26 AT→TA and GC→CG mutations that did not contribute to the bias; Table S3). For convenience, in simulations we used the fraction of GC→AT mutations = 0.55 and the fraction of AT→GC mutations = 0.35, thus obtaining WT GC→AT bias = 0.61.

Measuring growth rate as a fitness proxy

We measured growth rates of evolved isolates with single mutations and their respective ancestors in liquid culture media: LB broth (Miller, Difco), or M9 minimal salts (Difco) + 5 mM carbon source (glucose, trehalose, fructose, lactose, maltose, galactose, succinate, pyruvate, melibiose, fumarate, malate gluconate, mannose, N-acetyl-D-glucosamine (NAG), or glucuronate; Sigma-Aldrich). We inoculated each isolate from its freezer stock into M9 minimal salts medium with 0.4% glucose, and allowed it to grow at 37 ºC with shaking at 200 rpm for 16 hrs. We inoculated 6 µL of this culture into 594 µL growth media in 48-well plates (Costar) and incubated in a shaking tower (Liconic) at 37 ºC. Plates were read by an automated growth measurement system (Tecan, Austria) every 35-45 minutes for 18 hrs. We measured the growth rate of three technical replicates per isolate per growth medium; meaningful biological replicates could not be obtained since we had a single colony at the end of each MA line. The technical replicates were inoculated in the same microplate and measured on the same day. In each 48-well plate, we included the WT ancestor to estimate variation in growth rates across plates. We estimated maximum growth rate using the Curve Fitter software (68). Measurements across different days were highly repeatable (Fig. S1 in (29)) and measurements of the Δ*mutY* and WT ancestors in 12 environments were strongly correlated across two different years (in both cases, $R^2 > 0.99$, $p < 10^{-11}$).

For each evolved isolate, we used the average growth rate of three technical replicates to calculate relative growth rate as: Growth rate of evolved strain/Growth rate of ancestral strain. For WT MA lines, we used the WT ancestor; and for mutator MA lines, we used the mutator ancestor. The fitness effect of each mutation (s) is then calculated as relative growth rate –1, which is equivalent to (Growth Rate_{evo} – Growth Rate_{anc})/Growth Rate_{anc}. Usually, $s < 0$ indicates a deleterious

mutation, while s > 0 indicates a beneficial mutation (*s*>0). However, the estimated error in measurement of growth rates across technical replicates (run on the same day) was at most 5%. Hence, we conservatively considered mutants with *s* > –0.05 and *s* < 0.05 as showing no change in fitness, or neutral. We also tried using a different method to calculate fitness effects (selection coefficients) of mutations, following (69): $s = ((\text{Growth Rate}_{evo} - \text{Growth Rate}_{anc})/\text{Growth Rate}_{anc})*\ln 2$. We used *s* values of mutations to construct strain- and environment-specific distributions of fitness effects (DFE).

Correcting DFEs to account for selection bias during mutation accumulation

We corrected for selection bias during mutation accumulation as described recently (31). First, we corrected for selection bias in the MA environment (i.e., LB) for both WT and mutator. We binned observed fitness values in LB into 17 bins with a width of 0.05, to correspond with the maximum measurement error. Using the mean *s* value for each bin, we calculated the selection bias *b(s)* according to equation 2 (31). We used the τ value of 27 divisions per cycle of colony growth (i.e., per transfer in the MA experiment) as previously reported (29). We re-weighted each fitness bin by multiplying the bin frequency by $w = 1/b(s)$ to obtain the corrected frequencies in each bin. Finally, we normalized the corrected re-weighted frequencies as described in equation 3 (31).

Next, we corrected the DFEs in "new" environments (i.e., the 15 M9-minimal medium environments) according to equation 4 in (31). For each mutation, we used its fitness in LB to determine its weight $w_m = 1/b(s)$. Next, we binned fitness effects in the "new" environment into 17 bins, as done above for LB. In each bin, we calculated the sum of the w_m values for all mutations whose fitness effects fell into that bin. Finally, taking these summed w_m values as bin weights, we calculated bin frequencies, and re-normalized bin heights to sum to unity, as described above for LB. We performed these bias corrections for DFEs of both WT and mutator in each of the 15 new environments. The calculations are shown in the Supplementary Data file.

Estimating expected genetic load and supply of beneficial mutations

We calculated the deleterious load and supply of beneficial mutations for each strain as described earlier (45). Briefly, using the fraction of beneficial and deleterious mutations from the bias-corrected DFEs of WT and mutator, we calculated genetic load due to deleterious mutations as:

$$L_d = f_d N \mu$$

where L_d = deleterious genetic load; f_d = fraction of deleterious mutations; N = number of sites (here, *E. coli* genome size, 4.64×10^6 bp); μ = average genome-wide mutation rate of each strain (bp^{-1} $generation^{-1}$; Table S3). Similarly, we calculated the supply of beneficial mutations as:

$$S_b = f_b N \mu$$

where S_b = beneficial supply and f_b = fraction of beneficial mutations. Using the L_d and S_b values for each strain, we calculated the fold change in beneficial supply and genetic load of the mutator relative to WT. Next, we calculated the mutator L_d and S_b assuming that the WT and mutator DFEs were identical, and allowing for variation only in μ, as done in previous studies:

$$S_{b(\text{WT DFE})} = f_{b(\text{WT})} N \mu_{\Delta mutY}$$

$$L_{d(\text{WT DFE})} = f_{d(\text{WT})} N \mu_{\Delta mutY}$$

To measure the impact of accounting for the mutator's distinct DFE, we compared the fold change in the mutator's S_b and L_d values compared to WT, with or without assuming distinct DFEs. All calculated values are given in Tables S4 and S5.

Measuring the incidence of pleiotropy among new single mutations

We estimated the incidence of pleiotropy among new single mutations in the mutator (Δ*mutY*) background, as reported earlier for single mutations in WT *E. coli* (29). Briefly, for each possible pair of environments (total 210 pairs, given 15 minimal medium environments), we calculated the proportion of new mutations that increased fitness in one environment while decreasing fitness in another (antagonistic pleiotropy), simultaneously increased or decreased fitness in both environments (synergistic pleiotropic increases or decreases), changed fitness only in one environment, or did not change fitness in either environment. For each focal environment, we then calculated the mean proportion of each type of pleiotropic effect (considering all pairs that included that environment).

Next, we tested whether the differences in proportions of pleiotropy between WT and mutator could be recapitulated solely by shifting the WT DFE towards more beneficial mutations ("WT-beneficial shift"). We calculated the difference in median fitness effects of mutator and WT in each environment, and added this value to each of the WT fitness effects in that environment. The resulting DFE had a median equivalent to the mutator DFE, but retained the shape of the WT DFE. Similarly, we generated a WT DFE shifted towards more deleterious mutations ("WT-deleterious shift") by subtracting the same value from the relative fitness values of WT mutations. We used these "shifted" DFEs to calculate the proportion of fitness effects showing each type of (pairwise) pleiotropy. Finally, to measure pleiotropic effects across multiple environments, we counted the number of environments in which each mutation had a consistent effect (either beneficial or deleterious); and tested whether the proportion of mutations with consistent effects differed significantly across WT and mutator.

Estimating the effect of mutation spectrum changes via simulations of adaptive walks

We used an established evolutionary model to test whether and to what extent changes in mutation spectra are generally expected to affect the DFE. Following Stoltzfus (47), we simulated adaptive walks on the NK fitness landscape (28), modelling sequences composed of strings of four bases (A, C, G, T), allowing mutations to be classified as transitions or transversions, GC→AT or AT→GC, and so on. We used neighbourhood sizes of K=1 to 8, corresponding to relatively smooth and relatively rugged fitness landscapes. Each locus in the sequence was randomly assigned K neighbours from among all loci in the model. The fitness contribution of locus i (ω_i) depends on the state of that locus and the state of its neighbours. To create the fitness landscape when K=1, for each locus, 4^2 = 16 possible values of ω_i were drawn from a uniform distribution on (0,1); these values define ω_i if the state of the locus and its neighbour are AA, AC, AG... through TT. The fitness of the sequence (W) is then given by the sum of contributions from each locus, $W = \sum_{i=1}^{N} \omega_i$. When N=200, each landscape contained 4^{200} = 2.58 x 10^{120} unique sequences and fitness values. Increasing K increases the number of local fitness peaks; for example, when N=20 and K=8, the landscape has approximately 7000 distinct local peaks (70). For computational efficiency we simulated adaptive walks (strong-selection weak-mutation regime) rather than full populations. We

speculate that by allowing access to rare beneficial mutations of large effect, the benefit of bias shifts would be even further enhanced in clonal interference regimes.

When simulating Tv bias, starting at a randomly chosen resident (ancestor) sequence, we chose a single locus at random for mutation. The mutation is a transition with probability Ts and a transversion with probability Tv = 1 – Ts. Note that within transversions, each of the two possible outcomes (e.g. A→C or A→T) is chosen uniformly at random. The selective effect of the mutation was computed as $s = W_{mu}/W - 1$, where W_{mu} is the fitness of the mutant sequence, and W is the fitness of the current population sequence. The mutant sequence replaces the population sequence (a "step" in the walk occurs) with probability 2s if s > 0. The mutation spectrum (value of Ts) does not change during the adaptive walk. To investigate higher degrees of epistasis (more rugged landscapes), we varied both N and K, simulating adaptive walks and DFEs for N=8, 20 and 200, with K = 1-8 (Fig. S8).

We also implemented an alternative mutation scheme to test if the results varied for GC→AT biased mutation spectra. In these simulations, mutations were constrained such that 10% were AT→TA or GC→CG (mimicking our WT), and of the remaining mutations, fraction *x* were AT→GC, while (0.9-*x*) were GC→AT. For this mutation scheme, GC bias was calculated as the fraction of AT→GC mutations among all AT→GC or GC→AT mutations.

Inferring past evolutionary changes in mutation spectra

From previously published and our own mutation accumulation studies, we tabulated the predicted effects of the loss of 11 genes encoding DNA repair enzymes on the mutation spectrum, focusing on the Tv bias and GC→AT bias. To determine the evolutionary history of these genes, we detected orthologues and mapped predicted gain and loss events for each gene across the bacterial phylogeny, as described previously (48). Briefly, we pruned a previously described whole genome phylogeny based on >400 proteins (71) to generate a tree that included 1093 fully sequenced bacteria (48). Next, we downloaded the reviewed sequences for each DNA repair enzyme gene from UniProt, built a Hidden Markov Model (72), and searched for significant

orthologues in the genomes of the 1093 bacteria. Finally, we noted the presence/absence of each gene in each extant genome and carried out ancestral reconstruction of gene state (presence/absence), to infer the enzyme state at all nodes in the phylogeny. We used stochastic character mapping (73) in the R package 'phytools' (74) with the following parameters: transition rate matrix determination – Bayesian MCMC, prior distribution on the root node of the tree – estimated, number of simulations – 500. These parameters allow the function to first estimate the probability of the ancestral state at the root of the tree, and then determine the transition rate matrix that best explains the gene presence/absence data at the tips. A stochastic map is constructed using this transition rate matrix, which gives the probability of each character state at every node in the phylogeny. The function was simulated 500 times, each generating a different transition rate matrix and probabilities at the nodes. To score evolutionary transitions in character states, we first assigned each node with a state based on an average posterior probability of >=0.7 for either presence or absence of the gene, and then determined the nodes where the states switched. We used the predicted evolutionary transitions to count the total number of gains and losses of each enzyme in the phylogeny.

Next, we used the inferred state of all enzymes at every node in the tree (including the eubacterial ancestor and the extant taxa) to estimate the Tv and GC→AT bias at each node, relative to WT *E. coli*. For this calculation, we scaled all relative bias values (Table S12) between -1 and +1, such that negative values indicated a bias in one direction (e.g. more Tv mutations compared to WT *E. coli*) while positive values indicated a bias in the other direction (e.g. more Ts mutations compared to WT *E. coli*). Where possible, we used experimental data on double or triple knockouts of DNA repair mutants (Table S12); otherwise, we assumed additive effects of the missing enzymes. For each of the 1093 lineages in the tree, we traced the change in bias over time, up to the extant taxon. We used these data to calculate the observed number and direction of changes in bias in each lineage, categorising them as "no change", "single change", "reinforcement" and "reversal" (see schematic in Fig. S9A).

To derive expected changes in bias based on chance, we extracted the 500 estimated transition rate matrices (describing inferred rates of enzyme state transitions) from the stochastic character mapping described above. We used the function 'sim.history' in the R package phytools [52] to run 20 forward simulations for each matrix, yielding a total of 10,000 evolutionary simulations where enzyme state transitions occurred with similar rates as observed, but at stochastically determined nodes in the phylogeny. We used the number and direction of mutation bias changes in each simulation to calculate the average proportion of lineages showing a given number of reversals (or other changes in mutation bias) expected by chance (Fig. S9B). Finally, we inferred past evolutionary transitions across a broader set of DNA repair enzymes (without associated experimental data on their effects on the mutation spectrum), as described above (Fig. S10).

Acknowledgements

We thank Shyamsunder Buddh, Brian Charlesworth, Deborah Charlesworth, Joachim Krug, Krushnamegh Kunte, Saurabh Mahajan, Christopher Marx, and Mukund Thattai for discussion; Joshua Miranda for assistance with MA experiments; and the NGS facility at the Bangalore Life Sciences Cluster. **Funding:** We acknowledge funding and support from the National Centre for Biological Sciences (NCBS-TIFR), the Council for Scientific and Industrial Research India (Senior Research Fellowship to MS), the University Grants Commission of India (Senior Research Fellowship to GDD), the Department of Science and Technology India (KVPY Fellowship to BAB), the Natural Sciences and Engineering Research Council of Canada (LMW), and the Wellcome Trust (GDD is supported by grant 210585/B/18/Z to Robert B. Russell; and DBT/Wellcome Trust India Alliance grant IA/I/17/1/503091 to DA). We also thank the International Centre for Theoretical Sciences (ICTS) for supporting the Bangalore School on Population Genetics and Evolution (code: ICTS/popgen2020/01), where this collaboration was initiated. **Competing interests:** Authors declare no competing interests. **Author contributions:** MS designed and conducted experiments, analysed data, and drafted the manuscript. GDD designed and conducted phylogenetic analyses. BAB conducted experiments and analysed data. LMW designed and conducted simulation analyses. DA conceived and designed experiments and phylogenetic analyses, analysed data, obtained funding, and wrote the manuscript. **Data and materials availability:** All data used for

experimental and phylogenetic analysis are available as Supplementary Information files. Genome sequences will be deposited in GenBank, and simulation code is available on Github (https://github.com/lmwahl/MutationSpectrum).

References

1. P. L. Foster, H. Lee, E. Popodi, J. P. Townes, H. Tang, Determinants of spontaneous mutation in the bacterium Escherichia coli as revealed by whole-genome sequencing. *Proceedings of the National Academy of Sciences of the United States of America*, 201512136–10 (2015).

2. A. A. M. A. Mamun, *et al.*, Identity and function of a large gene network underlying mutagenic repair of DNA breaks. *Science* **338**, 1344–1348 (2012).

3. R. Maharjan, T. Ferenci, Mutational signatures indicative of environmental stress in bacteria. *Molecular Biology and Evolution* **32**, 380–391 (2014).

4. D. Agashe, N. Shankar, The evolution of bacterial DNA base composition. *Journal of Experimental Zoology Part B: Molecular and Developmental Evolution* **322**, 517–528 (2014).

5. H. Long, *et al.*, Evolutionary determinants of genome-wide nucleotide composition. *Nature Ecology & Evolution* **48**, 582 (2018).

6. J. Bohlin, O. Brynildsrud, T. Vesth, E. Skjerve, D. W. Ussery, Amino acid usage is asymmetrically biased in AT-and GC-rich microbial genomes. *PLoS ONE* **8**, e69878 (2013).

7. A. Couce, *et al.*, Mutator genomes decay, despite sustained fitness gains, in a long-term experiment with bacteria. *Proceedings of the National Academy of Sciences of the United States of America* **259**, 201705887–10 (2017).

8. A. Stoltzfus, L. Y. Yampolsky, Climbing Mount probable: Mutation as a cause of nonrandomness in evolution. *Journal of Heredity* **100**, 637–647 (2009).

9. M. A. Streisfeld, M. D. Rausher, Population genetics, pleiotropy, and the preferential fixation of mutations during adaptive evolution. *Evolution* **65**, 629–642 (2010).

10. D. R. Rokyta, P. Joyce, S. B. Caudle, H. A. Wichman, An empirical test of the mutational landscape model of adaptation using a single-stranded DNA virus. *Nature Genetics* **37**, 441–444 (2005).

11. K. Gomez, J. Bertram, J. Masel, Mutation bias can shape adaptation in large asexual populations experiencing clonal interference. *Proc Royal Soc B* **287**, 20201503 (2020).

12. A. V. Cano, J. L. Payne, Mutation bias interacts with composition bias to influence adaptive evolution. *Plos Comput Biol* **16**, e1008296 (2020).

13. A. Stoltzfus, D. M. McCandlish, Mutational biases influence parallel adaptation. *Molecular Biology and Evolution* **34**, 2163–2172 (2017).

14. J. F. Storz, *et al.*, The role of mutation bias in adaptive molecular evolution: insights from convergent changes in protein function. *Philosophical Transactions of the Royal Society B: Biological Sciences* **374**, 20180238–10 (2019).

15. A. V. Cano, J. L. Payne, Mutation bias interacts with composition bias to influence adaptive evolution. *Biorxiv* **6**, 2020.02.20.957217 (2020).

16. A. Couce, J. R. Guelfo, J. Blázquez, Mutational spectrum drives the rise of mutator bacteria. *PLoS Genetics* **9**, e1003167 (2013).

17. J. L. Payne, *et al.*, Transition bias influences the evolution of antibiotic resistance in Mycobacterium tuberculosis. *PLoS Biology* **17**, e3000265-23 (2019).

18. A. Bachar, *et al.*, Point mutations in topoisomerase I alter the mutation spectrum in E. coli and impact the emergence of drug resistance genotypes. *Nucleic Acids Research* **48**, 761–769 (2019).

19. S. M. Leighow, C. Liu, H. Inam, B. Zhao, J. R. Pritchard, Multi-scale predictions of drug resistance epidemiology identify design principles for rational drug design. *Cell Reports* **30**, 3951-3963.e4 (2020).

20. T. Ferenci, Irregularities in genetic variation and mutation rates with environmental stresses. *Environmental Microbiology* **21**, 3979–3988 (2019).

21. V. Katju, U. Bergthorsson, Old trade, new tricks: Insights into the spontaneous mutation process from the partnering of classical mutation accumulation experiments with high-throughput genomic approaches. *Genome Biology and Evolution* **11**, 136–165 (2018).

22. L. Y. Yampolsky, A. Stoltzfus, Bias in the introduction of variation as an orienting factor in evolution. *Evolution and Development* **3**, 73–83 (2001).

23. R. P. Maharjan, T. Ferenci, A shifting mutational landscape in 6 nutritional states: Stress-induced mutagenesis as a series of distinct stress input–mutation output relationships. *PLoS Biology* **15**, e2001477-22 (2017).

24. D. Agashe, The road not taken: Could stress-specific mutations lead to different evolutionary paths? *PLoS Biology* **15**, e2002862-5 (2017).

25. A. Stoltzfus, R. W. Norris, On the causes of evolutionary transition:transversion bias. *Molecular Biology and Evolution* **33**, 595–602 (2016).

26. D. M. Lyons, A. S. Lauring, Evidence for the Selective Basis of Transition-to-Transversion Substitution Bias in Two RNA Viruses. *Mol Biol Evol* **34**, 3205–3215 (2017).

27. Z. Zou, J. Zhang, Are nonsynonymous transversions generally more deleterious than nonsynonymous transitions? *Mol Biol Evol* **38**, msaa200- (2020).

28. C. A. Macken, A. S. Perelson, Protein evolution on rugged landscapes. *Proceedings of the National Academy of Sciences of the United States of America* **86**, 6191–6195 (1989).

29. M. Sane, J. J. Miranda, D. Agashe, Antagonistic pleiotropy for carbon use is rare in new mutations. *Evolution* **72**, 2202–2213 (2018).

30. D.-E. Chang, *et al.*, Carbon nutrition of Escherichia coli in the mouse intestine. *P Natl Acad Sci Usa* **101**, 7427–7432 (2004).

31. L. M. Wahl, D. Agashe, Selection bias in mutation accumulation. *Biorxiv*, 2021.08.03.454915 (2021).

32. A. Eyre-Walker, P. D. Keightley, The distribution of fitness effects of new mutations. *Nature Reviews Genetics* **8**, 610–618 (2007).

33. M. Weng, *et al.*, Fitness effects of mutation in natural populations of Arabidopsis thaliana reveal a complex influence of local adaptation. *Evolution* (2020) https:/doi.org/10.1111/evo.14152.

34. C. Zeyl, J. A. DeVisser, Estimates of the rate and distribution of fitness effects of spontaneous mutation in Saccharomyces cerevisiae. *Genetics* **157**, 53–61 (2001).

35. D. W. Hall, S. B. Joseph, A High Frequency of Beneficial Mutations Across Multiple Fitness Components in Saccharomyces cerevisiae. *Genetics* **185**, 1397–1409 (2010).

36. S. B. Joseph, D. W. Hall, Spontaneous Mutations in Diploid Saccharomyces cerevisiae More Beneficial Than Expected. *Genetics* **168**, 1817–1825 (2004).

37. W. J. Dickinson, Synergistic Fitness Interactions and a High Frequency of Beneficial Changes Among Mutations Accumulated Under Relaxed Selection in Saccharomyces cerevisiae. *Genetics* **178**, 1571–1578 (2008).

38. L. Perfeito, L. Fernandes, C. Mota, I. Gordo, Adaptive mutations in bacteria: high rate and small effects. *Science* **317**, 813–815 (2007).

39. C. Kozela, M. O. Johnston, Effect of Salt Stress on Mutation and Genetic Architecture for Fitness Components in Saccharomyces cerevisiae. *G3 Genes Genomes Genetics* **10**, g3.401593.2020 (2020).

40. R. G. Shaw, F. H. S. and C. Geyer, C. Geyer, What fraction of mutations reduces fitness? A reply to Keightley and Lynch. *Evolution* **57**, 686–689 (2003).

41. J. W. Thatcher, J. M. Shaw, W. J. Dickinson, Marginal fitness contributions of nonessential genes in yeast. *Proc National Acad Sci* **95**, 253–257 (1998).

42. M. Imhof, C. Schlötterer, Fitness effects of advantageous mutations in evolving Escherichia coli populations. *Proc National Acad Sci* **98**, 1113–1117 (2001).

43. F. H. Shaw, C. J. Geyer, R. G. Shaw, A COMPREHENSIVE MODEL OF MUTATIONS AFFECTING FITNESS AND INFERENCES FOR ARABIDOPSIS THALIANA. *Evolution* **56**, 453–463 (2002).

44. R. G. Shaw, D. L. Byers, E. Darmo, Spontaneous Mutational Effects on Reproductive Traits of Arabidopsis thaliana. *Genetics* **155**, 369–378 (2000).

45. S. Wielgoss, *et al.*, Mutation rate dynamics in a bacterial population reflect tension between adaptation and genetic load. *Proceedings of the National Academy of Sciences* **110**, 222–227 (2013).

46. H. A. Orr, The population genetics of adaptation: The distribution of factors fixed during adaptive evolution. *Evolution* **52**, 935–949 (1998).

47. A. Stoltzfus, Mutation-biased adaptation in a protein NK model. *Molecular Biology and Evolution* **23**, 1852–1862 (2006).

48. G. D. Diwan, D. Agashe, Wobbling forth and drifting back: The evolutionary history and impact of bacterial tRNA modifications. *Molecular Biology and Evolution* **35**, 2046–2059 (2018).

49. J. A. Eisen, P. C. Hanawalt, A phylogenomic study of DNA repair genes, proteins, and processes. *Mutation research* **435**, 171–213 (1999).

50. J. B. Losos, Seeing the Forest for the Trees: The Limitations of Phylogenies in Comparative Biology: (American Society of Naturalists Address). *Am Nat* **177**, 709–727 (2011).

51. M. Sharda, A. Badrinarayanan, A. S. N. Seshasayee, Evolutionary and Comparative analysis of bacterial Non-Homologous End Joining Repair. *Genome Biol Evol* **12**, evaa223- (2020).

52. M. A. Phillips, J. L. Steenwyk, X.-X. Shen, A. Rokas, Examination of gene loss in the DNA mismatch repair pathway and its mutational consequences in a fungal phylum. *Genome Biol Evol*, evab219- (2021).

53. A. Couce, O. Tenaillon, Mutation bias and GC content shape antimutator invasions. *Nature communications* **10**, 3114–9 (2019).

54. K. Jain, A. James, Fixation probability of a nonmutator in a large population of asexual mutators. *Journal of Theoretical Biology* **433**, 85–93 (2017).

55. Y. Raynes, P. D. Sniegowski, Experimental evolution and the dynamics of genomic mutation rate modifiers. *Heredity* **113**, 375–380 (2014).

56. J. A. G, Diminishing returns from mutation supply rate in asexual populations. *Science* **283**, 404–406 (1999).

57. O. Tenaillon, B. Toupance, H. L. Nagard, F. Taddei, B. Godelle, Mutators, population size, adaptive landscape and the adaptation of asexual populations of bacteria. *Genetics* **152**, 485–493 (1999).

58. C. F. Gentile, S.-C. Yu, S. A. Serrano, P. J. Gerrish, P. D. Sniegowski, Competition between high- and higher-mutating strains of Escherichia coli. *Biology Letters* **7**, 422–424 (2010).

59. L. Notley-McRobb, S. Seeto, T. Ferenci, Enrichment and elimination of mutY mutators in Escherichia coli populations. *Genetics* **162**, 1055–1062 (2002).

60. I. Matic, *et al.*, Highly variable mutation rates in commensal and pathogenic Escherichia coli. *Science* **277**, 1833–1834 (1997).

61. E. Denamur, *et al.*, Evolutionary implications of the frequent horizontal transfer of mismatch repair genes. *Cell* **103**, 711–721 (2000).

62. J. E. LeClerc, B. Li, W. L. Payne, T. A. Cebula, High mutation frequencies among Escherichia coli and Salmonella pathogens. *Science* **274**, 1208–1211 (1996).

63. T. Baba, *et al.*, Construction of Escherichia coli K-12 in-frame, single-gene knockout mutants: the Keio collection. *Molecular Systems Biology* **2**, 2460–11 (2006).

64. L. C. Thomason, N. Costantino, D. L. Court, *E. coli genome manipulation by P1 transduction* (John Wiley & Sons, Inc., 2001).

65. H. Li, R. Durbin, Fast and accurate short read alignment with Burrows-Wheeler transform. *Bioinformatics* **25**, 1754–1760 (2009).

66. H. Li, *et al.*, The Sequence Alignment/Map format and SAMtools. *Bioinformatics* **25**, 2078–2079 (2009).

67. D. C. Koboldt, *et al.*, VarScan: variant detection in massively parallel sequencing of individual and pooled samples. *Bioinformatics* **25**, 2283–2285 (2009).

68. N. F. Delaney, *et al.*, Development of an optimized medium, strain and high-throughput culturing methods for Methylobacterium extorquens. *PLoS ONE* **8**, e62957 (2013).

69. L.-M. Chevin, On measuring selection in experimental evolution. *Biology Letters* **7**, 210–213 (2010).

70. B. Østman, C. Adami, "Predicting Evolution and Visualizing High–Dimensional Fitness Landscapes" in *Recent Advances in the Theory and Application of Fitness Landscapes*, Emergence, Complexity and Computation., H. R. and A. P. Engelbrecht, A. P. Engelbrecht, Eds. (Springer-Verlag Berlin, 2014), pp. 509–526.

71. N. Segata, D. Börnigen, X. C. Morgan, C. Huttenhower, PhyloPhlAn is a new method for improved phylogenetic and taxonomic placement of microbes. *Nature communications* **4**, 2304–11 (2013).

72. S. R. Eddy, A new generation of homology search tools based on probabilistic inference. *Genome informatics. International Conference on Genome Informatics* **23**, 205–211 (2009).

73. J. P. Bollback, SIMMAP: stochastic character mapping of discrete traits on phylogenies. *BMC Bioinformatics* **7**, 88 (2006).

74. L. J. Revell, phytools: an R package for phylogenetic comparative biology (and other things). *Methods in Ecology and Evolution* **3**, 217–223 (2011).

Figure 1. Mutator DFEs have a larger fraction of beneficial mutations than WT. Stacked bar plots show the observed proportion of beneficial, deleterious and neutral mutations in WT and mutator. Average values across environments are given in the key; asterisks indicate significant differences between WT and mutator f_b, colored to show the strain with higher f_b (Table S2).

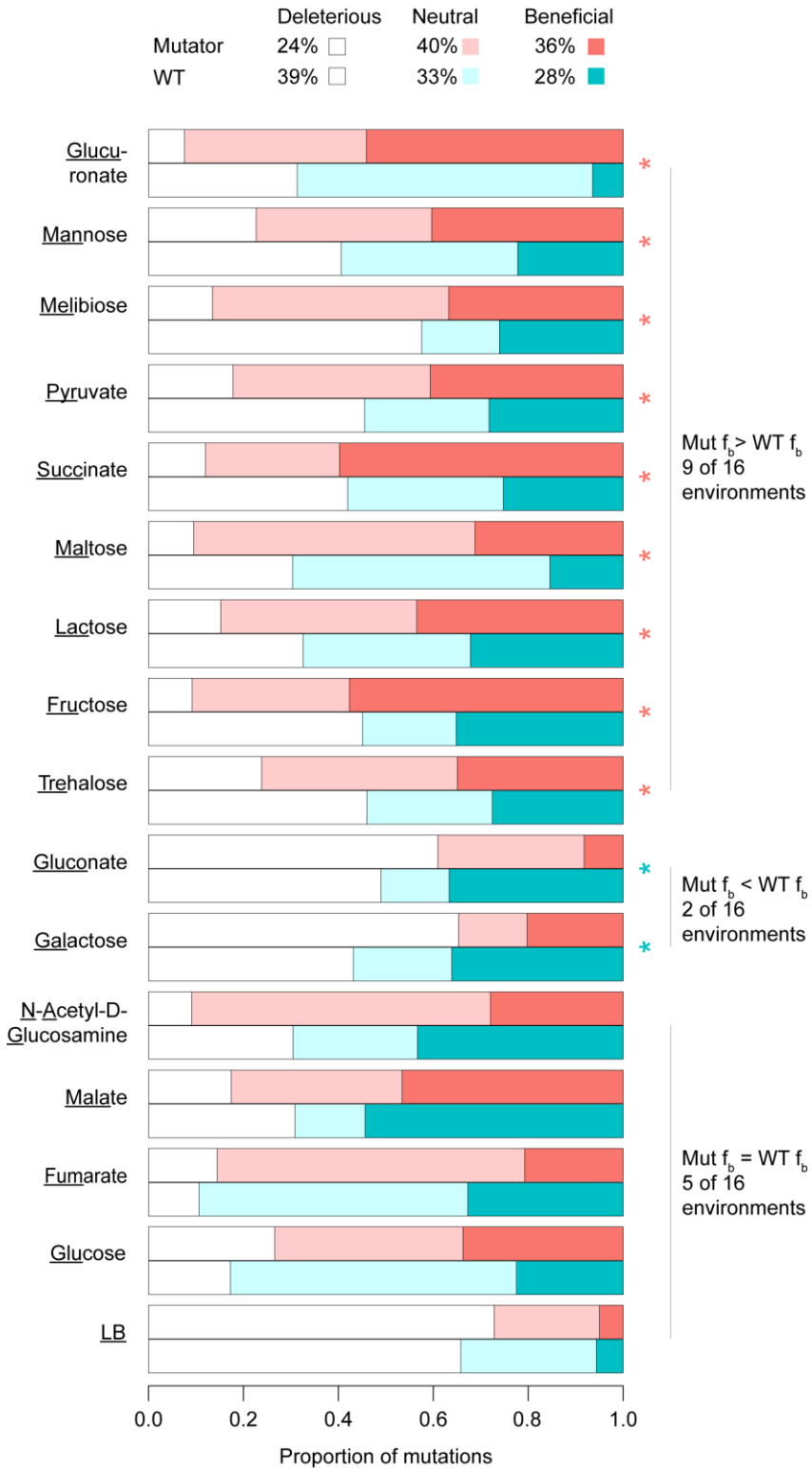

Figure 2. Beneficial-shifted DFE alters pleiotropic effects. (A) Schematic showing possible pleiotropic effects of mutations in two environments (W: relative fitness). (B–E) Median proportions of pleiotropic fitness effects of mutations in WT and mutator, and WT DFE artificially shifted towards either beneficial or deleterious mutations. Schematics indicate global DFEs (WT=cyan, mutator=pink, WT-shifted=light blue); black lines: relative fitness = 1. See Fig. S2B–E for proportions in each environment. (F) Pleiotropic effects of mutations across multiple environments. Frequency distributions show the proportion of mutations with consistent fitness effects (beneficial or deleterious) in a given number of environments. Black lines indicate medians.

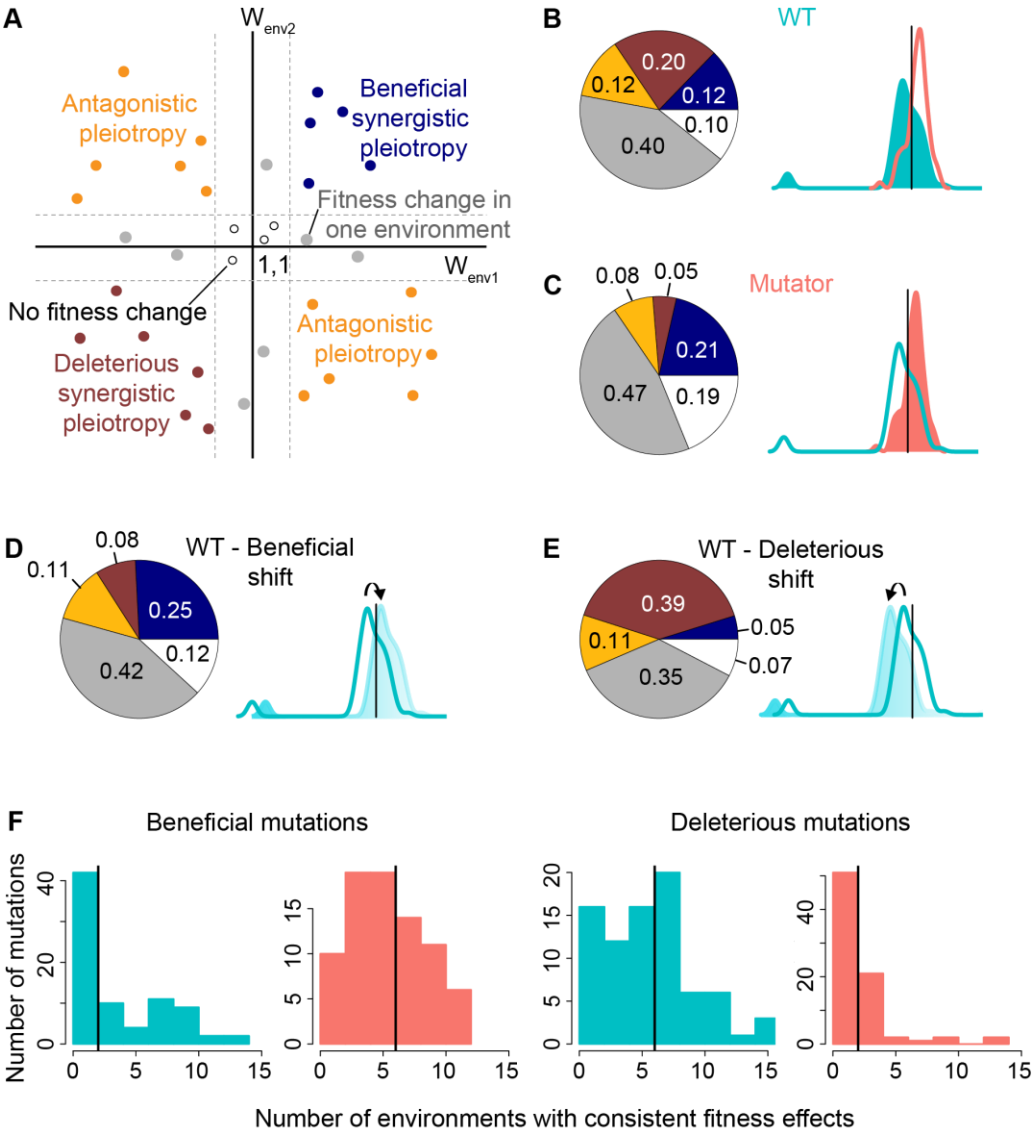

Figure 3. Differences in WT and mutator DFEs are best explained by differences in mutation spectra. (A) Growth rate of WT and mutator ancestors (n=12–24/strain/environment). Asterisks: significant differences between strains (Table S7). (B) Pairwise differences in the fitness effects of 19 mutations across genetic backgrounds (Mutator – WT); asterisks: significant difference from zero (black dotted line; Table S8). (C) Observed mutation biases in WT and mutator MA lines (including those with multiple mutations); the number of mutations of each type is noted. Asterisks: significant differences in proportions across strains (Table S3). (D–E) Fitness effects of different mutation classes, for MA-evolved isolates carrying single mutations. Boxplots (colored by strain and mutation class) show median, quartiles and range of relative fitness effects of mutations (open diamonds: outliers). Each boxplot was constructed with n x 16 data points (n = number of mutations, shown below each plot; pooled effects from 16 environments). Black horizontal lines: fitness impact = 0; asterisks: significant differences across mutation classes (Table S9); ns: not significant; nd: not determined.

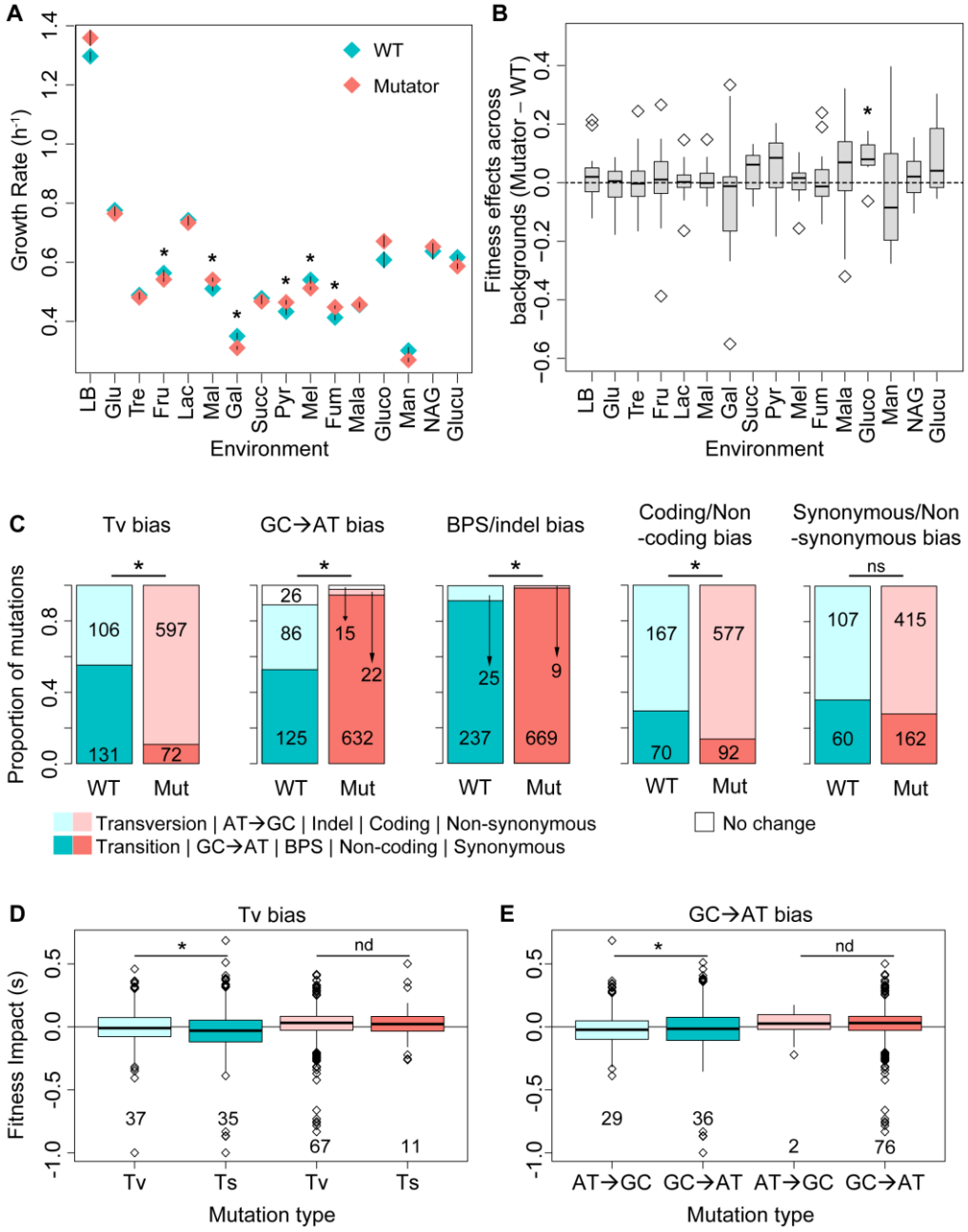

Figure 4. Simulations show general benefit of reversing mutation spectra. (A) Change in mean population fitness, fraction of beneficial and deleterious mutations (f_b and f_d), and mean magnitude of beneficial and deleterious effects (s_b and s_d) over the course of adaptive walks of a WT ancestor. (B) Impact of altering the WT mutation bias on f_b at different points along the adaptive walk (Tv bias = Tv/(Ts+Tv) mutations; grey dashed line: WT bias), as a function of the new mutation bias (shifted Tv bias). Line color: WT f_b at a given time; steeper lines (lighter colors): later evolutionary time, better adapted WT. (C–F) Waterfall plots show the impact of altering Tv bias (% change, shifted – WT) as a function of varying both WT (ancestor) and a strain with shifted bias, for a well-adapted WT population (f_b = 0.04). Each panel indicates the impact on different properties of the DFE: the fraction of beneficial or deleterious effects, and the mean fitness effect in each case. At a WT bias of 0.67, the impact of a bias shift is minimum; conversely, the maximum impact of bias shifts is observed for more extreme WT bias (close to 0 or 1) and an opposite extreme bias shift (close to 1 or 0). (G–H) Impact of introducing a mutation bias in an unbiased ancestor ("anc"), as a function of the new bias (shifted Tv or GC→AT bias). Panels show the results of simulations identical to those described in panel B, but starting with an unbiased ancestor.

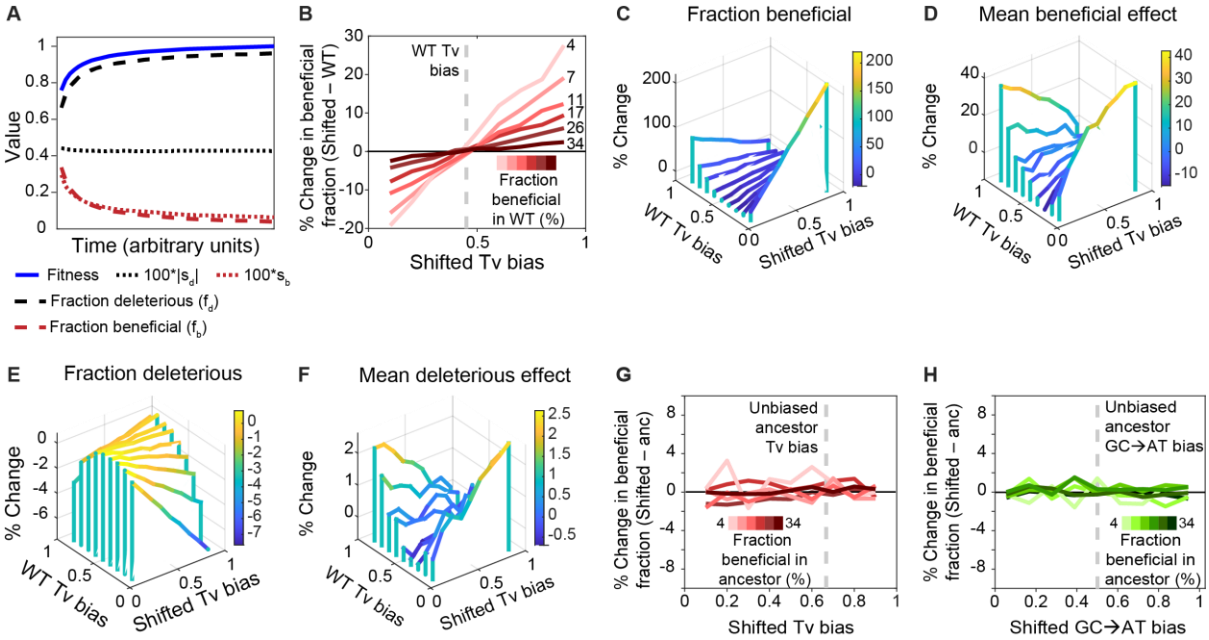
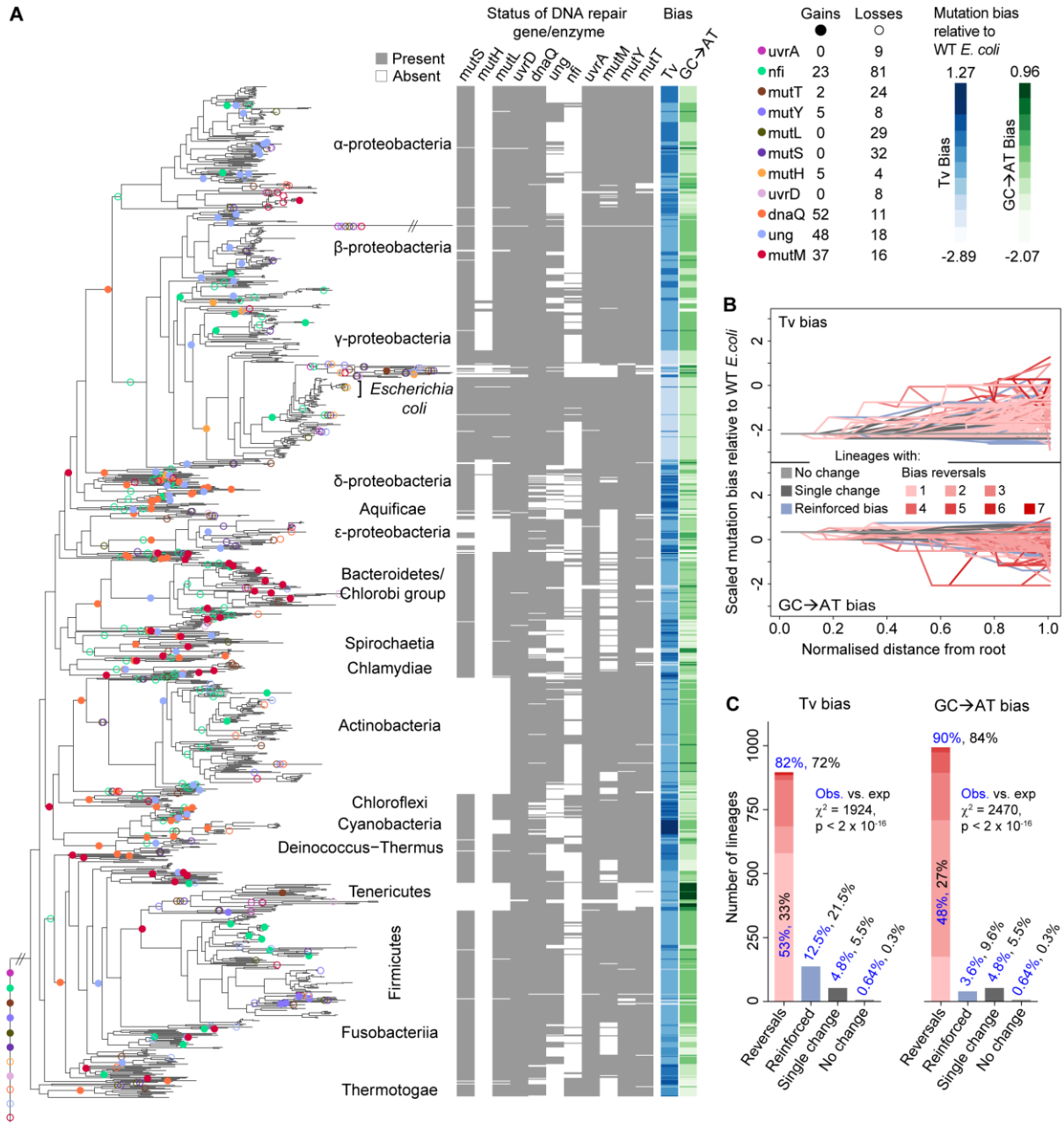
Figure 5. Phylogenetic analysis shows frequent evolutionary transitions in DNA repair genes and reversals in mutation spectra. (A) Patterns of gene presence/absence in extant taxa, used to map evolutionary transitions in DNA repair genes on the bacterial phylogeny (total transitions are shown in the key), and infer the magnitude of Tv and GC→AT biases relative to WT *E. coli* in extant taxa (heatmaps). (B) Inferred trajectories of mutational biases across 1093 lineages (C) Observed number of lineages showing spectrum shifts due to successive evolutionary transitions in repair enzymes (% values calculated as fraction across all lineages; blue=observed, black=expected values derived from stochastic forward simulations).